INDEX COPERNICUS INTERNATIONAL



Bio-Algorithms and Med-Systems

WWW.BAMSJOURNAL.COM ISSN: 1896-530X

ORIGINAL ARTICLE

Received: 14.09.2026
Accepted: 15.10.2026
Published: 31.10.2026

CITE THIS ARTICLE AS:
Kasperska K, Skurzok M, Moskal P. "Detection efficiency of two- and three-gamma positronium annihilations in the Total-Body J-PET detector," Bio-Algorithms and Med-Systems vol. 22, no. 2, pp. 1-9, 2026, DOI: 10.5604/01.3001.0055.9712

AUTHORS' CONTRIBUTION:
A – Conceptualization
B – Data Curation
C – Formal Analysis
D – Funding Acquisition
E – Investigation
F – Methodology
G – Project Administration
H – Resources
I – Software
J – Supervision
K – Validation
L – Visualization
M – Writing – Original Draft
N – Writing – Review & Editing

CORRESPONDING AUTHOR:
Kamila Kasperska MSc; Faculty of Physics, Astronomy and Applied Computer Science, Jagiellonian University, Kraków, Poland; E-mail: kamila.kasperska@doctoral.uj.edu.pl

COPYRIGHT:
Some rights reserved: Jagiellonian University Medical College. Published by Index Copernicus Sp. z o. o.

OPEN ACCESS:
The content of the journal „Bio-Algorithms and Med-Systems" is circulated on the basis of the Open Access which means free and limitless access to scientific data.

CREATIVE COMMONS CC, BY 4.0:
Attribution. It is free to copy, distribute, present and perform the copyrighted work and derivative works developed from it, provided that the name of the original author is cited.

Detection efficiency of two- and three-gamma positronium annihilations in the Total-Body J-PET detector

Kamila Kasperska[1,2,3ABCEFGIKLMN], Magdalena Skurzok[1,2AEFGJKMN], Paweł Moskal[1,2ADEFGHJKMN]

[1]Faculty of Physics, Astronomy and Applied Computer Science, Jagiellonian University, Kraków, Poland
[2]Center for Theranostics, Jagiellonian University, Kraków, Poland
[3]Jagiellonian University, Doctoral School of Exact and Natural Sciences, Kraków, Poland

ABSTRACT

Objective: We aimed to investigate the detection efficiency of two-gamma (2γ) and three--gamma (3γ) positronium annihilation events in the Total-Body J-PET (TB J-PET) detector and the influence of the energy-deposition threshold and annihilation position on the registration efficiency.
Materials: A realistic human body XCAT phantom was used to model the spatial distribution of positronium annihilations within the human body. The phantom was implemented in the simulated TB J-PET geometry.
Methods: Monte Carlo (MC) simulations were performed using GATE version 9.4.1 with the TB J-PET detector geometry. Para-positronium (p-Ps) and ortho-positronium (o-Ps) decays were simulated to represent 2γ and 3γ annihilation events, respectively. The detection efficiency was evaluated for energy-deposition thresholds of 0, 30 and 50 keV. Registered events were identified from the simulated photon interaction history and analysed according to their true point of origin within the phantom.
Results: The detection efficiency depended on the applied energy-deposition threshold and the point of origin within the phantom. The influence of the energy-deposition threshold differed between the 2γ and 3γ annihilation channels, resulting in changes in their registration efficiencies from 4.7% to 3.3% and from 1.11% to 0.22%, respectively, with efficiency ratios between the channels changing from 4.2 to 15.
Discussion: The different energy distributions of photons emitted in 2γ and 3γ decays led to different changes in detection efficiency with an increasing energy-deposition threshold. These differences should be considered when determining the 3γ/2γ annihilation rate ratio.
Conclusions: The results characterise the detection efficiency of 2γ and 3γ positronium annihilations in the TB J-PET geometry and aid the further development of quantitative 3γ/2γ imaging methods.

KEYWORDS

Positron Emission Tomography, Positronium imaging, Total-Body J-PET, Monte Carlo simulations, 3γ/2γ imaging

LIST OF ABBREVIATIONS

CT – computed tomography
GATE – Geant4 Application for Tomographic Emission
J-PET – Jagiellonian Positron Emission Tomography
MC – Monte Carlo
o-Ps – ortho-positronium
PET – positron emission tomography
PLI – positronium lifetime imaging
p-Ps – para-positronium
Ps – positronium
TB J-PET – Total-Body J-PET system
XCAT – eXtended CArdiac-Torso Phantom

BRIEF DESCRIPTION OF THE WORK

This study investigates the detection of two- and three-gamma positronium annihilation events in a Total-Body J-PET (TB J-PET) scanner using Monte Carlo (MC) simulations. Characterising the detection efficiency of both annihilation channels is important for the development of quantitative three-gamma/two-gamma positronium imaging and its potential future imaging applications.

INTRODUCTION

Positron emission tomography (PET) is one of the key medical imaging techniques, focused mainly on cancer diagnosis. During PET imaging, a patient is injected with a radiopharmaceutical labelled with a β^+-emitting radionuclide. The positrons annihilate directly with electrons from the body, emitting mainly two back-to--back photons with energies of 511 keV. The detection of the two photons allows the tomographic reconstruction of the radiotracer's concentration in the body [1, 2]. This imaging method forms a basis for PET and will be referred to in this work as two-gamma imaging.

Besides direct annihilation, positrons can form a metastable bound state with the electrons from the tissue, called a positronium (Ps), which exists in two spin states: singlet para-positronium (p-Ps) and triplet ortho-positronium (o-Ps). In a vacuum, p-Ps and o-Ps decay predominantly into two photons, with a mean lifetime of 125 ps, and three photons, with a mean lifetime of 142 ns, respectively [3]. However, o-Ps atoms in particular undergo additional processes in a medium, such as spin-exchange and pick-off annihilation, that change their decay channels [4]. Consequently, the o-Ps's lifetime is shortened, and the overall fraction of three-gamma (3γ) decays is lowered. How often these processes occur, and thus the properties of o-Ps, depend strongly on the tissue's sub-molecular structure [5, 6], leading to the development of the novel technique called positronium imaging [7–12].

The Jagiellonian Positron Emission Tomography (J-PET) group has demonstrated positronium lifetime imaging (PLI) in both ex vivo and in vivo studies [5, 12–17]. In parallel, the J-PET group is developing a Ps imaging method based on the 3γ to 2γ decay rate ratio, referred to as positronium ratio imaging [5, 18, 19]. A similar annihilation ratio-based approach is also being developed and demonstrated at the University of Tokyo [20, 21].

PLI is based on the so-called two-plus-one gamma imaging technique, which involves the detection of two back-to-back annihilation photons originating from the 2γ decay of Ps, together with an additional prompt gamma photon. The prompt photon is emitted during the nuclear de-excitation of the daughter nucleus, i.e., the nucleus formed by the radionuclide's β^+ decay, immediately following that decay. While the annihilation photons provide information about the time of Ps decay, the prompt gamma serves as a reference for determining the time of its formation. The time difference between these signals enables the determination of the Ps lifetime [15].

The $3\gamma/2\gamma$ decay rate ratio method is based on the detection of both types of annihilation events [18]. A key advantage of this method is that it does not require the detection of a prompt gamma. Consequently, it can be applied using a broader range of radionuclides, including the commonly used ^{18}F and the emerging ^{44}Sc isotope, which the J-PET group are planning to use [22, 23]. This approach is based on reconstructing the spatial distribution of the radiopharmaceutical concentration using both 2γ and 3γ annihilation events, the latter being reconstructed using the emerging 3γ imaging technique [24].

Both PLI [25–34] and 3γ imaging [21, 35–42] are emerging imaging techniques that have attracted increasing research interest in recent years. The first PLI [10, 12] and 3γ images [19, 21] have been successfully demonstrated.

Ps imaging is a promising extension of conventional PET, which enables the assessment of tissue properties beyond the spatial distribution of a radiopharmaceutical. Ps formed in a tissue is sensitive to its local environment and therefore provides information about tissue microstructure and chemical conditions. The $3\gamma/2\gamma$ decay rate ratio is particularly relevant, since the concentration of molecular oxygen influences o-Ps annihilation mechanisms [5]. The $3\gamma/2\gamma$ ratio may thus provide sensitivity not only to the size and concentration of the intermolecular voids but also to changes in tissue oxygenation. Importantly, simultaneous measurement of the mean o-Ps lifetime and its $3\gamma/2\gamma$ ratio may provide more reliable information than either parameter alone [5]. Both parameters are sensitive to the local environment of Ps, and their absolute values may vary significantly between different tissue types and between patients. However, their simultaneous measurement can reduce the bias from tissue heterogeneity and enable more specific assessment of oxygenation. This is particularly relevant, as hypoxia is associated with tumour aggressiveness and treatment resistance [5].

Photon attenuation in the patient's body is one of the major factors limiting the accuracy of both 2γ and 3γ image reconstruction. The attenuation of gamma rays in tissue leads to an underestimation of the radiotracer's concentration, particularly in deeper regions. Therefore, attenuation correction is essential for PET image

reconstruction. In the case of standard 2γ imaging, J-PET uses a CT-based attenuation correction technique [14, 43–45], and CT-less correction methods are under development [46]. However, the correction is more challenging for 3γ imaging, due to the continuous energy spectrum of the annihilation products [47, 48], requiring energy-dependent attenuation correction [49].

Photon absorption in anatomical human-body phantoms has previously been studied in Ref. [49]. The results were promising, as the absorption of photon triplets from 3γ decays was found to be only 2.5 times higher than that of the photon pairs from 2γ annihilations, suggesting the feasibility of 3γ imaging.

In this study, the analysis was extended by including the geometry of the TB J-PET system. The feasibility of 3γ imaging with TB J-PET by evaluating the efficiency of the 2γ and 3γ decays' registration was investigated, considering the detector's geometrical acceptance and the energy-deposition thresholds relevant for signal registration. The GATE MC simulation toolkit and an anatomical XCAT (eXtended CArdiac-Torso Phantom) phantom were employed. The results of this study present detection efficiency maps characterising the spatial dependence of photon registration efficiency for both 2γ and 3γ annihilation events.

MATERIALS AND METHODS

This study extends the previous investigation of photon attenuation effects in 2γ and 3γ decays of Ps, described in Ref. [49]. The phantom implementation, source generation, and the general simulation and data analysis workflow were adopted from that study, with the present study extending the simulations to include the geometry of the TB J-PET detector.

The simulations were carried out using GATE (Geant4 Application for Tomographic Emission), which is an open-source MC simulation framework developed by the OpenGATE Collaboration for medical imaging purposes [50]. GATE version 9.4.1 was used, which provides the capability to model complex multi-detector systems, making it suitable for reproducing the geometry of the TB J-PET detector. The simulations employed a J-PET-specific modification of GATE developed within the J-PET framework, which enabled accurate tracking of the three photons emitted in o-Ps decay and proper accounting for their interactions with the surrounding media [51]. GATE's ExtendedVSource library was used to generate o-Ps three-photon decays [50]. The decay kinematics were modelled according to the leading-order Ore–Powell model, as implemented in the underlying Geant4 G4OrePowellAtRestModel [52]. The decay points were sampled directly within the phantom; therefore, positron transport, positron range and Ps formation kinetics were not included in the simulations, while photon polarisation was not considered. The em_livermore_polar physics list was used to model the relevant electromagnetic interactions, including photoelectric absorption, Compton scattering and Rayleigh scattering. This physics list was routinely used in previous J-PET simulations.

The human body was modelled using the Mesh50_XCAT phantom developed by Auer et al. [53, 54]. The phantom represents a 50^{th}-percentile American male, with anatomical dimensions corresponding to the median values from the PeopleSize anthropometric database [55]. Its implementation, including the material assignment and voxelisation, followed the methodology described in Ref. [49]. In the present study, the head-only version of the phantom, comprising the head and neck regions, was used. Two separate sets of annihilation events, 2γ and 3γ, were simulated, with decay points sampled throughout the phantom.

The phantom was placed centrally inside the TB J-PET detector, with its longitudinal axis aligned with the axis of the detector. The full simulated volume of the phantom was enclosed within the detector's field of view. The TB J-PET geometry was implemented according to the description in Ref. [56] as shown in Fig. 1. The TB J-PET system consisted of five detector rings, each composed of 24 modules. Each module contained two layers of plastic scintillator strips, with 16 strips per layer. The scintillator strips had a cross-section of 30×6 mm^2. The system had two rings with 330 mm long scintillator strips and three rings with 600 mm long strips, providing an extended axial field of view of 254 cm, suitable for whole-body imaging. The inner radius of the detector was 414.7 mm, while the gap between adjacent detector rings was 2 cm.

The p-Ps and o-Ps sources were distributed uniformly throughout the voxelised phantom following the source generation procedure described in Ref. [49]. In total, 10^7 2γ decays and 4.435×10^7 3γ decays were simulated. The same event simulation workflow as in Ref. [49] was used, while the present study additionally accounted for the geometrical acceptance of the TB J-PET detector and investigated the effect of the applied energy-deposition thresholds on the registration efficiency of 2γ and 3γ events. The simulations were performed using the Polish high-performance computing infrastructure PLGrid, coordinated by ACK Cyfronet AGH.

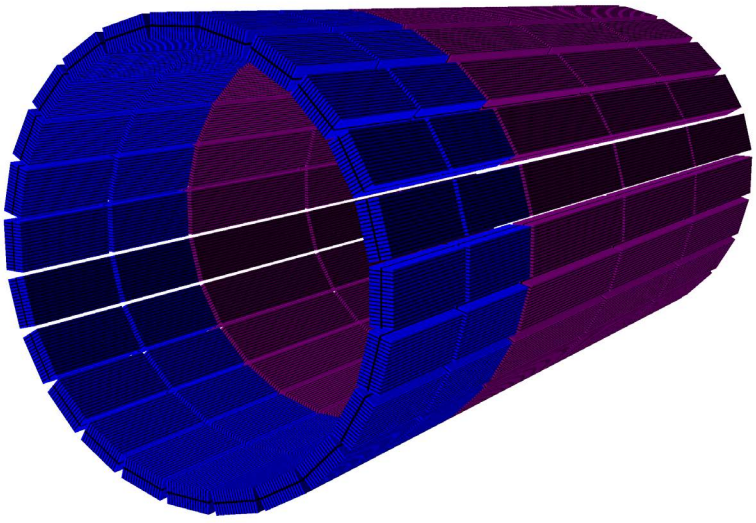


Fig. 1. Geometry of the Total-Body J-PET detector.

The simulated data were analysed using ROOT version 6.38.00 [57]. Events corresponding to true coincidences were identified based on the interaction history of the annihilation photons recorded by the GATE software. The following selection criteria were applied to each photon:

- The number of Compton scatterings in the phantom was equal to zero,
- The number of Rayleigh scatterings in the phantom was equal to zero,
- The number of Rayleigh scatterings in the detector was equal to zero,
- The number of Compton scatterings in the detector was equal to one.

The last criterion accounts for the fact that the dominant interaction mechanism of gamma photons with plastic scintillators is Compton scattering. A photon that underwent a single Compton scattering in the detector is considered registered, while events with more than one Compton interaction were classified as detector-scattered and therefore excluded from the analysis. The photons that did not interact with the detector at any stage, including those that were fully absorbed in the phantom, were not registered and consequently excluded from the analysis.

Following the event selection, the registered photons were grouped into pairs or triplets according to their common event ID, ensuring that the photons originated from the same decay. The analysis was performed for all events originating within the entire phantom and as a function of their points of origin within it. The point of origin was defined using the true decay position recorded by GATE rather than a position reconstructed from the detected photons. No annihilation point reconstruction was performed in this study. An additional angular selection was applied to the photon pairs and triplets, to further suppress events that did not satisfy the expected kinematic topology of Ps annihilation. The angles were calculated between vectors connecting the true annihilation position to the respective photon interaction positions in the detector. For 2γ events, pairs with an angle smaller than 179° between the photons were excluded. For 3γ events, only triplets where the sum of the three pairwise angles was equal to 360° were accepted. The resulting photon pairs and triplets were then counted to determine the number of registered 2γ and 3γ events. The above procedure was performed separately for the simulation data obtained with p-Ps and o-Ps sources.

RESULTS

The detection efficiencies of 2γ and 3γ events were evaluated for energy-deposition thresholds of 0, 30 and 50 keV. The overall detection efficiency was calculated as the ratio of the number of registered photon pairs or triplets to the total number of generated p-Ps or o-Ps decays, respectively. The resulting efficiencies for each energy threshold are summarised in Tab. I. The statistical uncertainties were below 0.2% for the p-Ps sample and below 0.4% for the o-Ps sample and were therefore negligible compared with the effects discussed in this study.

The spatial distribution of the detection efficiency was also determined. Efficiency maps were generated separately for the 2γ and 3γ decay channels and for each of the three energy-deposition thresholds. The resulting maps are presented in Fig. 2. and Fig. 3. and show the detection efficiency as a function of the decay position within the simulated phantom.

DISCUSSION

The reported simulations were performed to investigate the detection efficiency of 2γ and 3γ Ps decays in the TB J-PET detector, and to evaluate the influence of the energy-deposition threshold on the registration efficiency. The obtained results demonstrate that the registration efficiency depends on both the applied energy threshold and the location of the annihilation.

The comparison of the three energy-deposition thresholds shows that the detection efficiency of p-Ps gamma pairs is not affected significantly by the increasing energy threshold, while that of the o-Ps photon triplets drops significantly with increasing energy threshold. This effect is a result of the differences in the energy distributions of the emitted photons. In 2γ decays, both photons have a fixed energy of 511 keV, while the photon energies in 3γ decays follow a continuous distribution between 0 and 511 keV. Consequently, the resulting energy-deposition distributions for both channels extend continuously from 0 to approximately 340 keV but have different shapes (Fig. 4.). As the energy-deposition threshold is increased, different fractions of 2γ and 3γ events are therefore excluded, resulting in a different dependence of the detection efficiency on the threshold for the two annihilation channels.

The differences between the 2γ and 3γ detection efficiencies are particularly relevant for applications based on the $3\gamma/2\gamma$ annihilation--rate ratio. Since the ratio is determined from the numbers of

Tab. I. Detection efficiency of photon pairs or triplets originating from p-Ps and o-Ps decays, respectively, depending on the energy-deposition threshold. The detection efficiency is defined as a ratio of registered photon pairs or triplets to the generated number of p-Ps or o-Ps decays.

SOURCE	p-Ps			o-Ps		
Energy-deposition threshold [keV]	0	30	50	0	30	50
Detection efficiency [%]	4.7	3.8	3.3	1.11	0.42	0.22

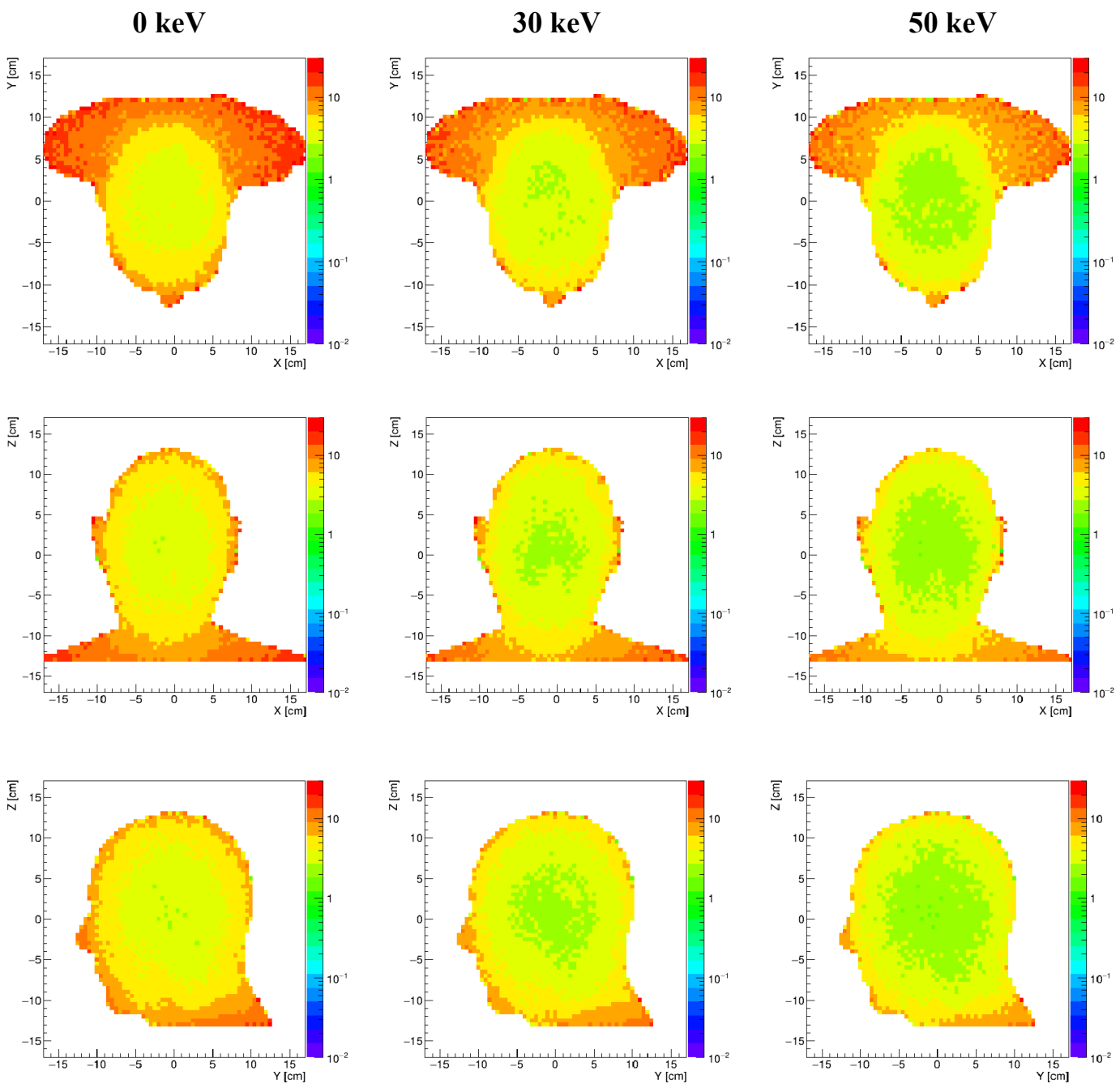


Fig. 2. Detection efficiency maps obtained for the 2γ p-Ps decays in the transverse, coronal and sagittal planes of the XCAT human body phantom, for the energy-deposition thresholds of 0, 30 and 50 keV. The efficiency is given in %. A logarithmic colour scale was used.

detected 2γ and 3γ events, differences in their detection efficiencies can introduce a spatial dependence into the measured ratio if they are not properly accounted for. The detection efficiency of the p-Ps decay photon pairs was observed to be approximately 4.2 to 15 times higher than the efficiency of o-Ps photon triplets. The contributions of photon absorption in the phantom, detector geometry and energy-deposition threshold can be assessed from the successive simulation stages. After accounting for photon transmission through the phantom, the efficiencies were 24.9% and 10.3% for p-Ps and o-Ps, respectively [49]. With a 0 keV energy-deposition threshold, the efficiencies decreased to 4.7% and 1.11%, corresponding to 18.9% and 10.8% of the events surviving the phantom, respectively. Increasing the threshold to 30 keV reduced the efficiencies to 3.8% for p-Ps and 0.42% for o-Ps, corresponding to 80.9% and 37.8% of their respective 0 keV efficiencies. At 50 keV, the efficiencies were further reduced to 3.3% and 0.22%, corresponding to 70.2% and 19.8% of the respective 0 keV efficiencies. These discrepancies were a result of both the higher absorption of the photon triplets in the phantom and the higher sensitivity of o-Ps triplets to the increases in the energy--deposition threshold. Both effects were the results of generally lower photon energies in the 3γ decays compared with the 2γ decays.

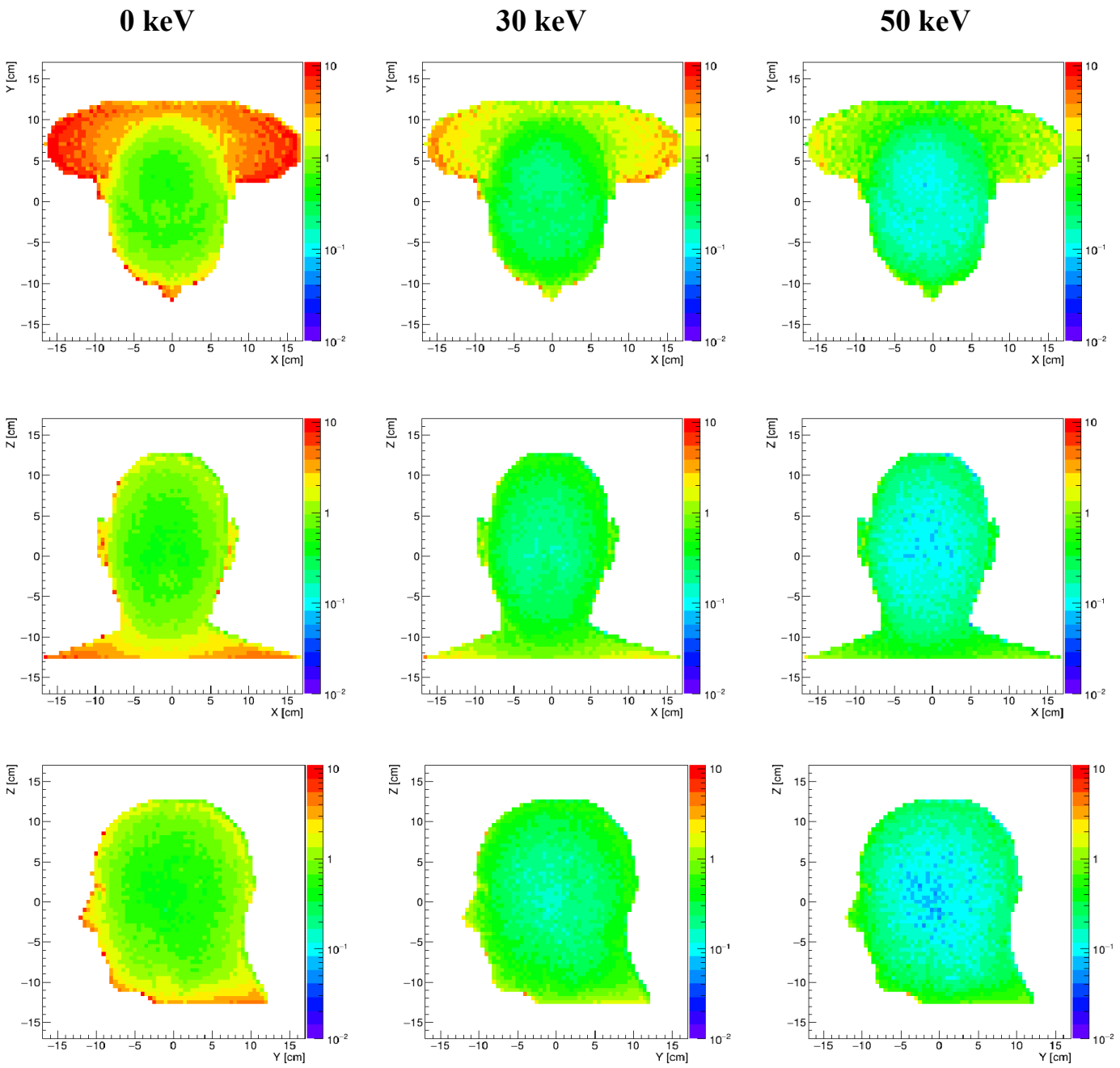


Fig. 3. Detection efficiency maps obtained for the 3γ o-Ps decays in the transverse, coronal and sagittal planes of the XCAT human body phantom, for the energy-deposition thresholds of 0, 30 and 50 keV. Efficiency is given in %. A logarithmic colour scale was used.

The present results extend the attenuation studies reported in Ref. [49] by incorporating the geometry of the TB J-PET detector. The use of a realistic human-body phantom together with the TB J-PET detector geometry provides a more realistic model of the conditions expected in whole-body Ps imaging. The results can therefore form a basis for further studies of the detection efficiency and for the development of correction techniques required for quantitative 3γ/2γ imaging.

The present study focused on the effects of detector geometry and the energy-deposition threshold on the detection efficiency of 2γ and 3γ events. The simulations did not include several aspects of the full detector response, such as detector timing, spatial and energy resolution. In addition, the analysis used the true annihilation positions provided by GATE, and no annihilation point reconstruction was performed. Therefore, the efficiency maps characterise the spatial dependence of the detection efficiency for the simulated data, rather than a complete image reconstruction procedure. Further studies should incorporate a more detailed model of the TB J-PET detector response and evaluate the influence of detector resolution and reconstruction algorithms on the detection efficiency and resulting spatial distributions.

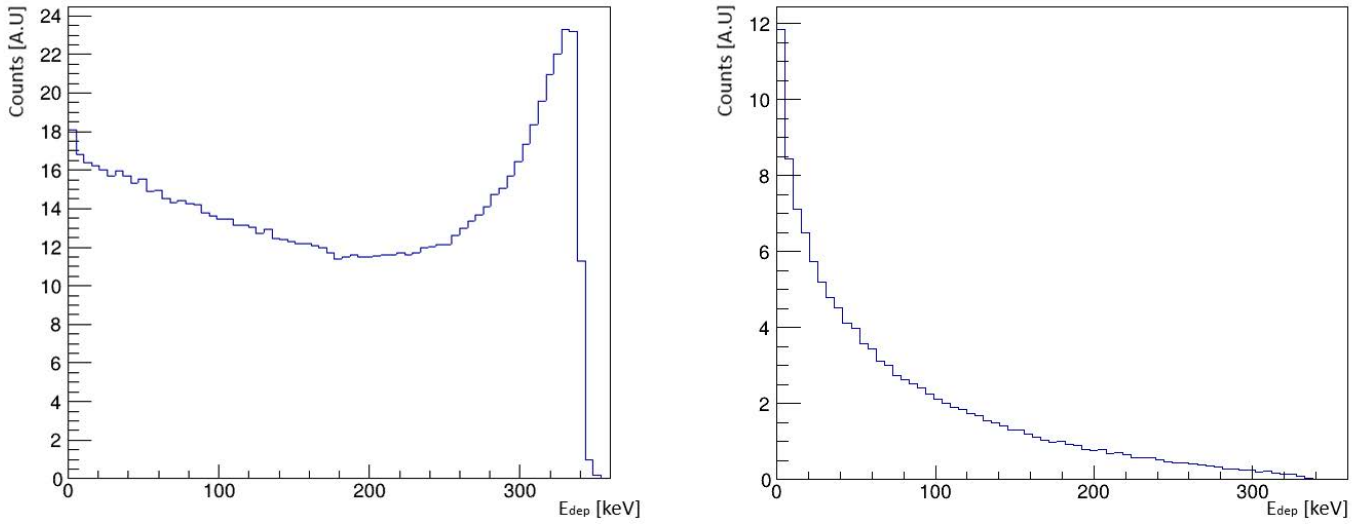


Fig. 4. Energy-deposition spectra of photons originating in 2γ decays (left) and 3γ decays (right).

CONCLUSIONS

This study investigated the detection efficiency of 2γ and 3γ Ps annihilation events in the TB J-PET detector using MC simulations with a realistic human body XCAT phantom. The influence of the energy-deposition threshold and the spatial position of the annihilation event on the registration efficiency was evaluated for both decay channels.

The results show that the detection efficiency depends on both the applied energy-deposition threshold and the point of origin within the phantom. The effect of the energy-deposition threshold also differs between the 2γ and 3γ decay channels. These differences in detection efficiency should be considered when determining the 3γ/2γ annihilation-rate ratio and in the development of quantitative decay-rate ratio Ps imaging methods.

The obtained efficiency distributions provide a basis for further studies of efficiency corrections and 3γ image reconstruction in the TB J-PET system. Future work should include a more complete model of the detector response, as well as incorporating the effects of both detector and image reconstruction resolution.

ACKNOWLEDGEMENTS

We acknowledge the Polish high-performance computing infrastructure PLGrid (HPC Centre: ACK Cyfronet AGH) for providing computer facilities and support within computational grant nos. PLG/2024/017688 and PLG/2025/018762.

CONFLICT OF INTEREST

Paweł Moskal holds patents for PET involving plastic scintillators and Ps imaging. Other authors declare no competing interests.

DATA AVAILABILITY

The data that support the findings of this study, the analysis software and the supplementary materials are all available from the corresponding author upon request.

CODE/SOFTWARE AVAILABILITY

The software used for the analysis is available from the corresponding author upon request.

FUNDING

We acknowledge support from the National Science Centre through grant nos. 2021/42/A/ST2/00423, 2021/43/B/ST2/02150, and 2022/47/I/NZ7/03112, the European Union within the Horizon Europe Framework Programme (ERC Advanced Grant POSITRONIUM no. 101199807), the SciMat and qLife Priority Research Areas budget under the programme Excellence Initiative Research University at Jagiellonian University, and the Research Support Module as part of the Excellence Initiative – Research University programme at Jagiellonian University.

REFERENCES

1. Humm JL, Rosenfeld A, Del Guerra A. From PET detectors to PET scanners. Eur J Nucl Med Mol Imaging. 2003;30(11):1574–97. doi: https://doi.org/10.1007/s00259-003-1266-2.
2. Zatcepin A, Ziegler SI. Detectors in positron emission tomography. Z Med Phys. 2023 Feb;33(1):4–12. doi: https://doi.org/10.1016/j.zemedi.2022.08.004.
3. Bass SD, Mariazzi S, Moskal P, Stępień E. Colloquium: Positronium physics and biomedical applications. Rev Mod Phys. 2023;95(2):021002. doi: https://doi.org/10.1103/RevModPhys.95.021002.
4. Tuomisto F, Barthe MF, Cizek J, Eijt SWH, Green DG, Gribakin GF, et al. Positron annihilation spectroscopy. Nat Rev Methods Primers. 2026;6(1):56. doi: https://doi.org/10.1038/s43586-026-00511-5.
5. Moskal P. Quantum Entanglement Degree, Mean Positronium Lifetime, and the 3γ/2γ Annihilation-Rate Ratio as Novel PET Biomarkers for Hypoxia – Concept, Challenges, and Predictions. Bio-Algorithms and Med-Systems. 2026;22(1):56–77. doi: https://doi.org/10.5604/01.3001.0055.7461.
6. Moskal P, Jasińska B, Stępień EŁ, Bass SD. Positronium in medicine and biology. Nat Rev Phys. 2019;1:527–9.
7. Moskal P. Positronium Imaging. 2019 IEEE Nuclear Science Symposium and Medical Imaging Conference (NSS/MIC), Manchester, UK, 2019, pp. 1–3, doi: 10.1109/NSS/MIC42101.2019.9059856.
8. Moskal P, Kisielewska D, Curceanu C, Czerwiński E, Dulski K, Gajos A, et al. Feasibility study of the positronium imaging with the J-PET tomograph. Phys Med Biol. 2019;64(5):055017. doi: https://doi.org/10.1088/1361-6560/aafe20.
9. Moskal P, Kisielewska D, Shopa R, Bura Z, Chhokar J, Curceanu C, et al. Performance assessment of the 2 γ positronium imaging with the total-body PET scanners. EJNMMI Phys. 2020;7(1):44. doi: https://doi.org/10.1186/s40658-020-00307-w.
10. Moskal P, Dulski K, Chug N, Curceanu C, Czerwiński E, Dadgar M, et al. Positronium imaging with the novel multiphoton PET scanner. Sci Adv. 2021;7(42):eabh4394. doi: https://doi.org/10.1126/sciadv.abh4394.
11. Moskal P, Bilewicz A, Das M, Huang B, Khreptak A, Parzych S, et al. Positronium Imaging: History, Current Status, and Future Perspectives. IEEE Trans Radiat Plasma Med Sci. 2025;9(8):981–1001. doi: https://doi.org/10.1109/TRPMS.2025.3583554.
12. Moskal P, Baran J, Bass S, Choiński J, Chug N, Curceanu C, et al. Positronium image of the human brain in vivo. Sci Adv. 2024;10(37):eadp2840. doi: https://doi.org/10.1126/sciadv.adp2840.
13. Das M, Mryka W, Beyene EY, Parzych S, Sharma S, Stępień E, et al. Estimating the efficiency and purity for detecting annihilation and prompt photons for positronium imaging with J-PET using toy Monte Carlo simulation. Bio-Algorithms and Med-Systems. 2023;19(1):87–95. doi: https://doi.org/10.5604/01.3001.0054.1938.
14. Das M, Reimund B, Sharma S, Parzych S, Niedźwiecki S, Badawi R, et al. Development of correction techniques for the J-PET Scanner. Bio-Algorithms and Med-Systems. 2024;20:1–8. doi: https://doi.org/10.5604/01.3001.0054.9362.
15. Das M, Sharma S, Beyene EY, Bilewicz A, Choinski J, Chug N, et al. First Positronium Imaging Using 44Sc With the J-PET Scanner: a Case Study on the NEMA-Image Quality Phantom. IEEE Trans. Radiat. Plasma Med. Sci. 2026;10(4):593–602. doi: https://doi.org/10.1109/TRPMS.2025.3621554.
16. Kubat K, Das M, Sharma S, Beyene EY, Bilewicz A, Choiński J, et al. First ex-vivo positronium imaging of tissues with modular J-PET scanner using 44Sc radionuclide. Z. für Med. Phys. 2026;36(3):357–65. doi: https://doi.org/10.1016/j.zemedi.2026.03.004.
17. Das M, Sharma S, Beyene EY, Bilewicz A, Choiński J, Chug N, et al. First positronium lifetime imaging using 52Mn and 55Co with a plastic-scintillator-based PET scanner. Sci Rep. 2026;16(1):16230. doi: https://doi.org/10.1038/s41598-026-43965-z.
18. Jasińska B, Moskal P. A New PET Diagnostic Indicator Based on the Ratio of 3γ/2γ Positron Annihilation. Acta Physica Polonica B. 2017;48:1577–82. doi: https://doi.org/10.5506/APhysPolB.48.1577.
19. Moskal P, Gajos A, Mohammed M, Chhokar J, Chug N, Curceanu C, et al. Testing CPT symmetry in ortho-positronium decays with positronium annihilation tomography. Nat Commun. 2021;12(1):5658. doi: https://doi.org/10.1038/s41467-021-25905-9.
20. Shimazoe K, Uenomachi M. Quantum sensing and imaging in the MeV regime of nuclear medicine. Appl Phys Express. 2026;19(4):040104. doi: https://doi.org/10.35848/1882-0786/ae5bde.
21. Fujimoto M, Sato R, Hamdan M, Uenomachi M, Caradonna P, Stephenson L, et al. Advancing PET through direct imaging of three-photon decay using pure positron emitters. Commun Phys. 2026;9(1):254. doi: https://doi.org/10.1038/s42005-026-02782-6.
22. Moskal P, Stępień E, Khreptak A. A vision to increase the availability of PET diagnostics in low- and medium-income countries by combining a low-cost modular J-PET tomograph with the 44Ti/44Sc generator. Bio-Algorithms and Med-Systems. 2024;20(Special Issue):55–62. doi: https://doi.org/10.5604/01.3001.0054.9273.
23. Moskal P, Stępień EŁ. Prospects and Clinical Perspectives of Total-Body PET Imaging Using Plastic Scintillators. PET Clinics. 2020;15(4):439–52. doi: https://doi.org/10.1016/j.cpet.2020.06.009.
24. Gajos A, Kamińska D, Czerwiński E, Alfs D, Bednarski T, Białas P, et al. Trilateration-based reconstruction of ortho-positronium decays into three photons with the J-PET detector. Nucl. Instrum. Methods Phys. Res. A. 2016;819:54–9. doi: https://doi.org/10.1016/j.nima.2016.02.069.
25. Takyu S, Nishikido F, Tashima H, Akamatsu G, Matsumoto K, Takahashi M, et al. Positronium lifetime measurement using a clinical PET system for tumour hypoxia identification. Nucl. Instrum. Methods Phys. Res. A. 2024;1065:169514. doi: https://doi.org/10.1016/j.nima.2024.169514.
26. Takyu S, Shibuya K, Nishikido F, Tashima H, Takahashi M, Yamaya T. Two-dimensional positronium lifetime imaging using certified reference materials. Appl Phys Express. 2022;15(10):106001. doi: https://doi.org/10.35848/1882-0786/ac8d7b.
27. Takyu S, Ikeda H, Wakizaka H, Nishikido F, Matsumoto K, Tashima H, et al. Positron annihilation lifetime measurement with TOF-PET detectors: feasibility of Iodine-124 use. Appl Phys Express. 2023;16(11):116001. doi: https://doi.org/10.35848/1882-0786/ad047c.
28. Mercolli L, Steinberger WM, Grundler PV, Moiseeva A, Braccini S, Conti M, et al. First positronium lifetime imaging with scandium-44 on a long axial field-of-view PET/CT. Front Nucl Med. 2025;5:1–8. doi: https://doi.org/10.3389/fnume.2025.1648621.
29. Mercolli L, Steinberger WM, Rathod N, Conti M, Moskal P, Rominger A, et al. Phantom imaging demonstration of positronium lifetime with a long axial field-of-view PET/CT and 124I. EJNMMI Phys. 2025;12(1):80. doi: https://doi.org/10.1186/s40658-025-00790-z.
30. Huang B, Wang Z, Zeng X, Goldan AH, Qi J. Fast high-resolution lifetime image reconstruction for positron lifetime tomography. Commun Phys. 2025;8(1):181. doi: https://doi.org/10.1038/s42005-025-02100-6.
31. Huang B, Li T, Arino-Estrada G, Dulski K, Shopa RY, Moskal P, et al. SPLIT: Statistical Positronium Lifetime Image Reconstruction via Time-Thresholding. IEEE Trans Med Imaging. 2024;43(6):2148–58. doi: https://doi.org/10.1109/TMI.2024.3357659.

32. Qi J, Huang B. Positronium Lifetime Image Reconstruction for TOF PET. IEEE Trans Med Imaging. 2022;41(10):2848–55. doi: https://doi.org/10.1109/TMI.2022.3174561.

33. Huang B, Dai B, Lapi SE, Liles G, Karp JS, Qi J. High-Resolution Positronium Lifetime Tomography at Clinical Activity Levels on the PennPET Explorer. J Nucl Med. 2025;66(9):1464–70. doi: https://doi.org/10.2967/jnumed.125.270130.

34. Huang HH, Zhu Z, Booppasiri S, Chen Z, Pang S, Kao CM. A statistical reconstruction algorithm for positronium lifetime imaging using time-of--flight positron emission tomography. IEEE Trans Radiat Plasma Med Sci. 2025;9(4):478–86. doi: https://doi.org/10.1109/trpms.2025.3531225.

35. Tashima H, Yamaya T. Three-Gamma Imaging in Nuclear Medicine: A Review. IEEE Transactions on Radiation and Plasma Medical Sciences. 2024;8(8):853–66. doi: https://doi.org/10.1109/TRPMS.2024.3470836.

36. Kacperski K, Spyrou NM, Smith FA. Three-gamma annihilation imaging in positron emission tomography. IEEE Transactions on Medical Imaging. 2004;23(4):525–9. doi: https://doi.org/10.1109/TMI.2004.824150.

37. Abuelhia E, Kacperski K, Kafala S, M Spyrou N. Performance of triple coincidence imaging as an addition to dedicated PET. Radiat. Phys. Chem. 2007;76(2):351–6. doi: https://doi.org/10.1016/j.radphyschem.2006.03.066.

38. Kacperski K, Spyrou NM. Performance of three-photon PET imaging: Monte Carlo simulations. Phys Med Biol. 2005;50(23):5679. doi: https://doi.org/10.1088/0031-9155/50/23/019.

39. Abuelhia E, Kacperski K, Spyrou NM. Three-photon annihilation in PET: 2D imaging experiments. J Radioanal Nucl Chem. 2007;271(2):489–95. doi: https://doi.org/10.1007/s10967-007-0235-9.

40. Abuelhia E, Alzimami K, Alkhorayef M, Podolyák Z, Spyrou NM. Measurement of coincidence timing resolution of scintillation detectors compared to semiconductor detectors to image three-photon positron annihilation. J Radioanal Nucl Chem. 2008;278(3):767–71. doi: https://doi.org/10.1007/s10967-008-1608-4.

41. Yu Z, Asch H, Gerber R, Redey A, Starosta K, Tam D, et al. Novel application of the 8π gamma-ray spectrometer for 3γ positron emission tomography. Nucl. Instrum. Methods Phys. Res. A. 2026;1084:1–7. doi: https://doi.org/10.1016/j.nima.2025.171168.

42. Alkhorayef M, Sulieman A, Alsager OA, Alrumayan F, Alkhomashi N. Investigation of using positronium and its annihilation for hypoxia PET imaging. Radiat. Phys. Chem. 2021;188:109690. doi: https://doi.org/10.1016/j.radphyschem.2021.109690.

43. Bayerlein R, Das M, Sharma S, Badawi RD, Beyene EY, Chug N, et al. Monte Carlo-based scatter correction for the plastic-based modular PET scanner J-PET. Phys Med Biol. 2026;71(7):075026. doi: https://doi.org/10.1088/1361-6560/ae54fb.

44. Ay MR, Sarkar S. Computed tomography based attenuation correction in PET/CT: Principles, instrumentation, protocols, artifacts and future trends. Iran. J. Nucl. Med. 2007;15(2):1–29.

45. Carney JPJ, Townsend DW, Rappoport V, Bendriem B. Method for transforming CT images for attenuation correction in PET/CT imaging. Med Phys. 2006;33(4):976–83. doi: https://doi.org/10.1118/1.2174132.

46. Tiwari S, Sharma S, Moskal P. Feasibility Study of Using Detector-Scattered Photons for Attenuation Correction in CT-less PET Imaging. Bio-Algorithms and Med-Systems. 2025;21(Special Issue):13–20. doi: https://doi.org/10.5604/01.3001.0055.4655.

47. Adkins GS. Analytic evaluation of the amplitudes for orthopositronium decay to three photons to one-loop order. Phys Rev A. 2005;72(3):032501. doi: https://doi.org/10.1103/PhysRevA.72.032501.

48. Skurzok M, Bass SD, Kasperska K, Beyene E, Chug N, Curceanu C, et al. Experimental determination of the Dalitz plot for positronium decay using the J-PET detection system. Phys Lett B. 2026;882:141018. doi: https://doi.org/10.1016/j.physletb.2026.141018.

49. Kasperska K, Skurzok M, Moskal P. Studies of Attenuation Effects in Two- and Three Photon Positronium Decays in Phantom Models. Bio-Algorithms and Med-Systems. 2025;21(Special Issue):42–51. doi: https://doi.org/10.5604/01.3001.0055.5414.

50. Jan S, Santin G, Strul D, Staelens S, Assié K, Autret D, et al. GATE: a simulation toolkit for PET and SPECT. Phys. Med. Biol. 2004;49:4543–61.

51. Raedler M. Gate, v9.4.1_cluster, GitHub repository [Internet]. [cited 2026 Oct 6]. Available at: https://github.com/mraedler/Gate/tree/v9.4.1_cluster.

52. Geant4 Collaboration. Decays of orthopositronium at rest to 3 photons. Physics Reference Manual [Internet]. [cited 2026 Oct 6]. Available at: https://geant4.web.cern.ch/documentation/dev/prm_html/PhysicsReferenceManual/decay/OrthoPositronium.html.

53. Auer B, Könik A, Fromme TJ, De Beenhouwer J, Kalluri KS, Lindsay C, et al. Mesh modelling of system geometry and anatomy phantoms for realistic GATE simulations and their inclusion in SPECT reconstruction. Phys Med Biol. 2023;68(7):075015. doi: https://doi.org/10.1088/1361-6560/acbde2.

54. Auer B. Mesh-based-Human-Phantom-for-Simulation [Internet]. [cited 2026 Sept 4]. Available at: https://github.com/BenAuer2021/Mesh-based-Human-Phantom-for-Simulation.

55. Open Ergonomics – Anthropometrics Data [Internet]. [cited 2026 Sept 4]. Available at: https://openerg.com/.

56. Ardebili KT, Beyene EY, Chug N, Curceanu C, Czerwiński E, Das M, et al. Development of a Cost-Effective Total Body J-PET From Plastic Scintillators: Definitive Design. In: 2025 IEEE Nuclear Science Symposium (NSS), Medical Imaging Conference (MIC) and Room Temperature Semiconductor Detector Conference (RTSD) [Internet]; 1–8 Nov 2025; Yokohama, Japan. IEEE; 2025. p. 1–2. doi: https://doi.org/10.1109/NSS/MIC/RTSD57106.2025.11287221.

57. Brun R, Rademakers F. ROOT – An object oriented data analysis framework. Nucl. Instrum. Methods Phys. Res. A. 1997;389(1–2):81–6. doi: https://doi.org/10.1016/S0168-9002(97)00048-X.